Strain hardening behaviour in sintered Fe–0.8%C–1.0%Si–0.8%Cu powder metallurgy preform during cold upsetting

A Rajeshkannan* and **S Narayan**
Mechanical Engineering, The University of the South Pacific, Suva, Fiji

The manuscript was received on 1 April 2009 and was accepted after revision for publication on 3 June 2009.

DOI: 10.1243/09544054JEM1587

Abstract: Cold upsetting experiments were performed on sintered Fe–0.8%C–1.0%Si–0.8%Cu steel preforms in order to evaluate the strain hardening characteristics. Powder preforms of 86 per cent theoretical density and an initial aspect ratio of 0.4 were prepared using a suitable die and a 1 MN capacity hydraulic press. Sintering was carried out in an electric muffle furnace for a period of 90 min at 1150 °C. Each sintered compact was subjected to an incremental compressive loading of 0.04 MN until fractures appeared on the free surface. Experiments were performed with no lubricant and using graphite as a lubricant. The behaviour of the applied stress as a function of both strain and densification level exhibits a continuous enhancement over three different response modes. The first and third stage responses offer a high resistance to deformation, whereas the second stage shows virtually steady-state behaviour. The instantaneous strain hardening exponent n_i and strength coefficient K_i of the steel preforms were calculated and found to continuously increase with an increase in the deformation and densification levels.

Keywords: cold upsetting, applied stresses, strain, densification, strain hardening

1 INTRODUCTION

Powder metallurgy (PM) processing is a net- or near net-shape manufacturing technology, which in many instances removes the need for extensive secondary machining operations [**1**]. The parts produced by PM methods are also unique and innovative [**2**]. For example, PM processing is used to fabricate the low alloy steel parts used for structural and load bearing purposes in automobiles and off-road vehicles [**3**]. Powder preform upsetting involves the fabrication of a preform using a conventional PM processing technique, followed by the forging of the preform to its final shape, this involves substantial densification [**4**]. In upsetting operations, the induced height strain can lead to lateral flow of the PM preform material. Thus, a spherical pore in the preform would undergo flattening and simultaneous elongation in the direction of the lateral flow, which is normal to the direction of loading. This leads to the situation where a relative motion between the opposite sides of the pore, due to the presence of shear stress, becomes feasible and mechanical rupturing of the oxide film on the metal surface takes place. Virgin metal is thus exposed for bond formation across the collapsing pore surfaces. It has been established [**5**, **6**] that the flow of material during upsetting and densification produces fibring of inclusions in the lateral direction.

Cold upsetting of a porous PM material consists of both ductile fracture and strain hardening. These two mechanisms determine the feasibility of the powder upsetting operations and help to achieve high-quality final products. Ductile fracture is the common mode of failure, it is a complex phenomenon that is dependent on both process and material parameters. The ductile properties of metals have been extensively investigated by many researchers [**7**, **8**]. During cold working operations the powders in a preform experience not only the usual strain hardening,

**Corresponding author: Mechanical Engineering, School of Engineering and Physics, Faculty of Science and Technology, The University of the South Pacific, Laucala Campus, PO Box 1168, Suva, Fiji.*
email: narayanan_su@usp.ac.fj

phenomenon but also geometrical strain hardening, due to a continued increase in the density which leads to an increase in cross-sectional area. Thus, the total strain hardening in PM preforms is the result of the densification and cold working of the base material surrounding the pores [**9**, **10**]. It has been clearly established that an increase in the volume of the voids decreases the relative critical pressure and vice versa [**11**]. However, closing and opening of the voids occurs with tri-axial compression and tension respectively, with the absolute values of the relative critical pressure being the same in both cases. Whenever the relative critical pressure is exceeded, a void of given geometry begins to open faster than it would close under tri-axial compression of the same magnitude [**12**]. The factors determining the geometry change of the pore are the pattern and the level of the plastic deformation [**13**]. Thus, it is obvious that the start and continuation of pore closure can be accomplished at a comparatively lower pressure when the material is subjected to plastic deformation.

In frictionless upsetting tests for sintered PM preforms, the deformation is uniform, showing no barrelling of the cylindrical surface [**14**]. The study of barrelling in PM cylindrical preforms under axial deformation is described in [**15**]. A decrease in the aspect ratio along with an increase in friction levels at contact surfaces increases the curvature of the bulged surface. A non-uniform deformation in the presence of frictional forces results in the existence of secondary tensile stresses in the circumferential direction accompanying the axial compressive stresses [**16**]. Since, the primary cause of fracture in upsetting is tensile stresses, it is therefore essential to investigate fracture during the deformation processing of sintered powder materials with the help of axial upsetting tests.

The primary objective of the present investigation is to determine the effects of friction conditions on the relationship between applied compressive stress with continuous deformation and densification, and also the strain hardening behaviour during cold upsetting of sintered Fe–0.8%C–1.0%Si–0.4%Cu PM preforms.

2 EXPERIMENTAL DETAILS

Atomized iron powder with a 150 μm grain size was obtained from Sundaram Fasteners Limited, Hyderabad, India. Silicon and copper powders each with a 37 μm grain size were obtained from the Metal Powder Company, Thirumangalam, Madurai, Tamil Nadu, India, and graphite powder with a grain size of 2–3 μm was supplied by Ashbury Graphite Mills Inc., Ashbury Warren County, New Jersey, USA. Analysis indicated that the purity of the iron, copper, and silicon powders was 99.7, 99.93, and 99.90 per cent respectively with the insoluble impurities accounting for the remaining fractions. The characteristics of the iron powder and Fe–0.8%C–1.0%Si–0.8%Cu blend are shown in Tables 1 and 2.

The required amount of powder corresponding to the investigated system was measured and blended in a pot mill along with porcelain balls in a ratio of 1:1 by weight for a period of 20 h in order to obtain an homogeneous mix. This powder blend was compacted using a 1 MN hydraulic press using a pressure of 480 ± 10 MPa to obtain an initial density of 0.86 ± 0.01 of the theoretical density. These green compacts were sintered in an electric muffle furnace at 1150 ± 10 °C for 90 min. In order to avoid oxidation during sintering, the compacts were coated with a ceramic [**17**]. These sintered preforms were furnace cooled.

The sintered and furnace-cooled preforms were machined to yield a constant height-to-diameter ratio of 0.40 and were compressively deformed between a flat die – set under an incremental loading step of 0.04 MN using the 1 MN capacity hydraulic press under two different frictional conditions, namely, no lubrication and the use of a graphite lubricant. Dimensional measurements such as the deformed height and deformed diameters (including bulged and contact) were carried out after every deformation step and density measurements were performed using the Archimedes principle [**18**]. The experimental results were used to calculate the

Table 1 Characterization of iron powder and Fe–0.8%C–1.0%Si–0.8%Cu blend

Si. number	Property	Iron	Fe–0.8%C–1.0%Si–0.8%Cu blend
1	Apparent density (g/cc)	2.96	2.91
2	Flowrate (s/100 g), measured using a Hall flow meter	56.0	47.4
3	Compressibility (g/cc) at pressure of 430 ± 10 MPa	6.55	6.64

Table 2 Sieve size analysis of the iron powder

	Sieve size (μm)									
	+150	+126	+106	+90	+75	+63	+53	+45	+37	−37
Wt% ret.	10.14	21.90	9.46	2.02	20.10	12.10	11.10	5.70	0.31	7.00

engineering stress, true stress, true height strain, percentage theoretical density, instantaneous strength coefficient (K_i) and instantaneous strain hardening exponent (n_i).

3 RESULTS AND DISCUSSION

3.1 Stress–strain characteristics

Stress–strain analysis is considered to be the most appropriate technique to assess the mechanical behaviour of a material when it is subjected to any form of external loading condition. This is because it allows the internal resistance of a material to an external disturbance at a particular cross-sectional area exposed to the deformation force to be determined. Strain normally deals with the deformation of the body. When the applied incremental load is directly considered at the original cross-sectional diameter D_0, i.e. before deformation, it is called the engineering stress, and when the same applied incremental load is considered at the instantaneous deformed diameter D_f, it is called the true stress. Since both the stresses are a result of the applied load, they can be labelled as applied stresses, and can be plotted against the true height strain to assess the resistance to deformation for the induced height strain during cold axial forging as is shown in Fig. 1. From this figure it can be concluded that an increasing height strain, results in increasing stresses. The resistance to the deformation is clearly desirable during the first stage (up to the value of 0.05 height strain) and has effectively ceased in the last stage (after approximately the value of 0.6 height strain); however, the intermediate stage exhibits a relatively steady and constant increase in the stress values. This reveals the fact that the 14 per cent porosity in the preform at the initial stage cannot be deformed by the initial application of an incremental loading; however, this loading stimulates the particle kinetics: both voids and materials. However, this is not true in the last stage because the porosity level is lower, approximately 4–5 per cent (refer to Fig. 2,) and thus the preforms are significantly densified.

In addition, extensive induced strains make the preform densify more, and the small amount of pores would be expected to behave as a second phase during the deformation as is often encountered in fully dense materials (as in the production of ingots). Thus, in addition to a height reduction, lateral deformation is also pronounced. This is the cause of the lower true stress value in comparison with engineering stress values and also the reason why it does not exist in the last stage. The lateral spread is distinct after a height strain value of 0.1 as can be observed in Fig. 1. This indicates that in the intermediate or

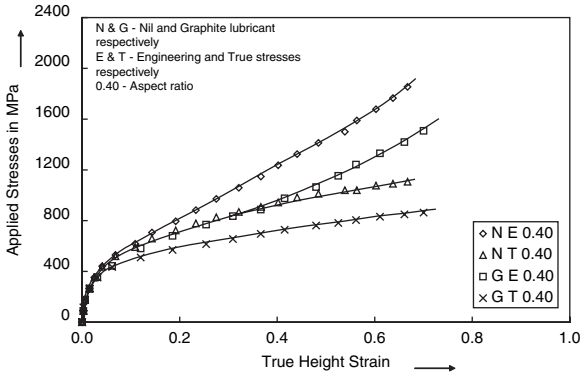

Fig. 1 Influence of lubrication conditions on the relationship between applied stresses and true height strain

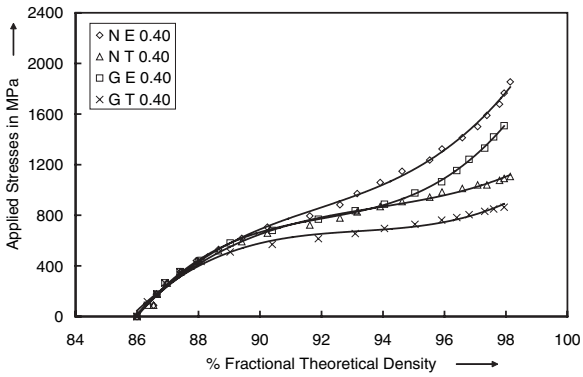

Fig. 2 The influence of lubrication conditions on the relationship between the applied stress and density

second stage, where the induced strain contributes to increase the particle kinetics and reduce the slope of the applied stress curves, the resistance offered to deformation is considerably lower than in the first and last stages. This behaviour is true whether or not a lubricant is used during the deformation.

3.2 Stress–densification characteristics

It is well-established [**19**, **20**] that densification can be appreciably enhanced by the application of one or more deformation processes; therefore, densification is a function of induced strain. Similarly, the strength and other mechanical properties are highly dependent on the maximum density of the PM preform and of course, the mode by which full densification is attained. Generally speaking, strength can be expressed as the resistance against deformation up to the fracture point. Therefore, strength is also a function of the density. Thus, experiments were performed to find out the relationship between the applied stresses and the density obtained during continuous cold forging. The corresponding plot is shown in Fig. 2. The characteristics of the curves follow similar trends, and consist of three different stages as was observed in Fig. 1. Also, detailed

observation of the figure reveals the existence of a third stage for the true stress against densification plot. This was not seen in the true stress against height strain plot. At initial stages (from initial pack density to 88 per cent of the theoretical density), the applied load is not sufficient to deform the preform and so there is only a small rise in the stress values. Continued application of the load leads to the collapse of bigger pores since these pores are more sensitive to stress concentration, and then the collapse of smaller pores and pore beds. This results in higher densification levels in the preform, which in turn increases the applied stress values. However, the slope of the second stage is relatively shallow in comparison to the first stage which confirms the significant role of the kinetics or mobility of the particles.

The critical observation from Fig. 2 is that a divergence between the values of the engineering and true stresses, irrespective of the use of lubricants, starts virtually at the end of the first stage. This means that until the end of the first stage, specimen height reduction is high and lateral expansion is low. As soon as an 88–89 per cent of theoretical density level is achieved, the deformation in both linear and lateral directions is appreciable. This effect is not as pronounced in the last stage with high densification levels, i.e. between 95 per cent of theoretical density and the maximum densification that can be achieved. The reason for the steeper slope seen for the last stage especially for engineering stress values is that the material is expected to strain harden due to the induced strain during cold forging. However, the presence of voids and their deformation along with the material in the lateral direction lowers the true stress values in order to bear the applied load. Furthermore, at any value of the attained densification, it can be observed that preforms deformed under dry conditions experience higher stress values than preforms deformed under lubricated conditions. This indicates that the use of a graphite lubricant facilitates the lateral deformation of the preform and results in lower densification levels in comparison with dry conditions. This is because friction between the die and preform surfaces induces a transverse pressure, which reinforces the vertical forming pressure and enhances the densification of the material. The magnitude of the lateral pressure increases with an increase in the friction level.

3.3 Theoretical description

Based on the nature of the applied stress against induced strain and densification plots, it cannot be claimed that strength was also induced in a preform during the cold deformation. Even though the stress rise is substantial for engineering stress as a function of densification level, this is not a true behaviour. Therefore, an attempt was made to use the plastic flow (Ludwik) equation $\sigma = K\varepsilon^n$, with suitable modification for PM performs, to determine the instantaneous strength (K_i) and instantaneous strain hardening (n_i), where σ is the true stress, ε is true strain, K is strength coefficient, and n is the strain hardening exponent [**21**].

The consecutive applied loads on the preform are specified as 1, 2, 3, . . . , $m-1$, m. The plastic flow equation can be written as

$$\sigma_m = K\varepsilon_m^n \tag{1}$$

$$\sigma_{m-1} = K\varepsilon_{m-1}^n \tag{2}$$

Subtracting equations (1) and (2), the following expression can be obtained

$$\sigma_m - \sigma_{m-1} = K(\varepsilon_m^n - \varepsilon_{m-1}^n) \tag{3}$$

Then equation (3) can be further reduced to

$$K_i = \frac{\sigma_m - \sigma_{m-1}}{\varepsilon_m^n - \varepsilon_{m-1}^n} \tag{4}$$

Now, dividing equation (1) by equation (2), the following expression is obtained

$$\frac{\sigma_m}{\sigma_{m-1}} = \frac{\varepsilon_m^n}{\varepsilon_{m-1}^n} = \left(\frac{\varepsilon_m}{\varepsilon_{m-1}}\right)^n \tag{5}$$

Taking the natural logarithm of both sides of equation (5), leads to

$$\ln\left(\frac{\sigma_m}{\sigma_{m-1}}\right) = n\ln\left(\frac{\varepsilon_m}{\varepsilon_{m-1}}\right) \tag{6}$$

Equation (6) can be further simplified to

$$n_i = \frac{\ln(\sigma_m/\sigma_{m-1})}{\ln(\varepsilon_m/\varepsilon_{m-1})} \tag{7}$$

Equations (4) and (7) can be utilized to determine the instantaneous strength coefficient and instantaneous strain hardening exponent from the corresponding experimental data on the stress and strain levels.

3.4 Strain hardening characteristics

Figures 3 and 4 show the relationship between the instantaneous strength coefficient (K_i) and the true height strain and percentage fractional theoretical density respectively. It can be seen that between 35 and 40 per cent of the height strain and/or up to 94 per cent of theoretical density, the strength values fall at almost the same rate. After these points fluctuating behaviour is observed. This behaviour is more pronounced when a lubricant is not used during the deformation. In general, it is observed that as the induced height strain and densification increase, the instantaneous strength coefficients also

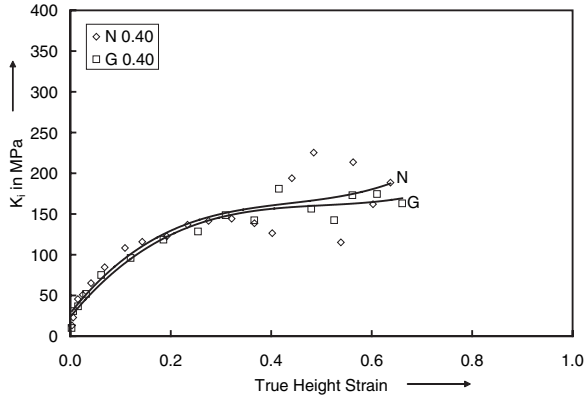

Fig. 3 The relationship between K_i and the true height strain, and the effect of using a lubricant

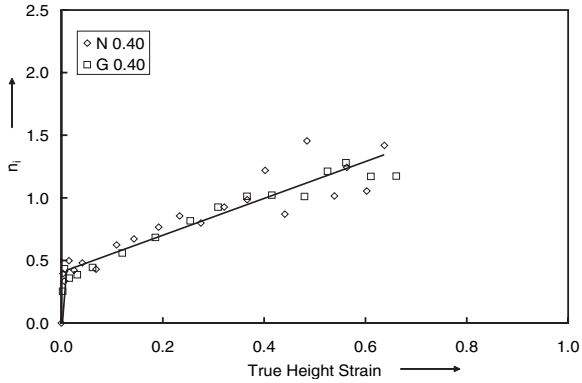

Fig. 5 The relationship between n_i and the true height strain and the effect of using a lubricant

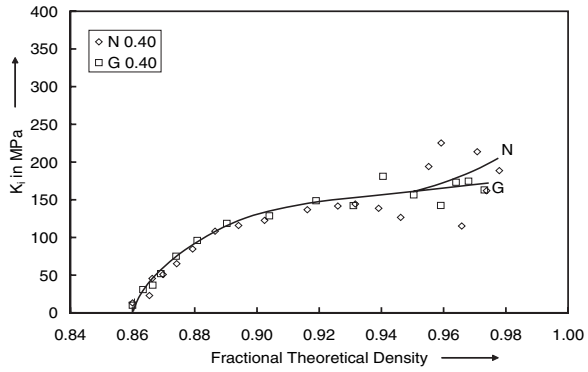

Fig. 4 The relationship between K_i and the percentage fractional theoretical density, and the effect of using a lubricant

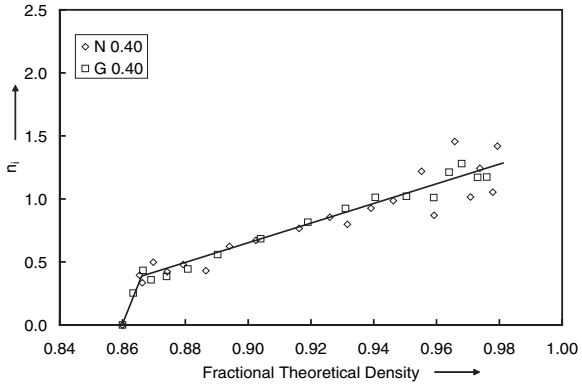

Fig. 6 The relationship between n_i and the percentage fractional theoretical density and the effect of using a lubricant

increase. This phenomenon can also be seen in Figs 1 and 2 where the applied stress values continuously increase with an increase in height strain and densification. However, a reason for the fluctuating behaviour could be that the deformation induced in the preform is not homogeneous or that the load distribution is not homogeneous during deformation and this becomes significant at later stages of the deformation. Thus, it can be concluded that an increase in friction levels between the die and preform will increase the fluctuations in the strength coefficient. However, approximate curves have been drawn to the fluctuating points, with the curve for the no lubricant case lying above the curve for the lubricated case. Furthermore, it can be concluded from these plots that irrespective of the use of lubricants, the strength can be continuously increased by continuous cold deformation and densification. However, a maximum strength level is reached for the preform deformed without the use of a lubricant.

Figures 5 and 6 show the instantaneous strain hardening exponent (n_i) as a function of the true height strain and fraction of the theoretical density respectively.

It can be seen from these figures that the strain hardening level continuously increases with increasing deformation level. The preform deformed without the use of a lubricant appears to strain harden slightly quicker than, the preform deformed using a lubricant, however, the latter has an extended deformation region before it begins to strain harden.

This can be understood by reference to Figs 5 and 6. From these figures it is clear that the measured points begin to be scattered more quickly in the case of no lubricant than for the use of graphite as a lubricant. This is proof that as soon as the rate of densification slows down because the mobility of particles becomes lower then the work hardening effect is promoted. It is noted that all the preforms were deformed until a crack appears at the free end and it is suggested that the identification of the point at which the fracture occurs can be utilized to introduce circumferential constraint to stop crack growth. This would yield a material with no pores and enhanced properties.

3.5 Microstructure

To further establish the cold deformation characteristics, preforms completely deformed under both lubricated and non-lubricated conditions were cut into two halves and the specimens were prepared for microstructural analysis. Micrographs were taken both at the centre and the edges of the specimens in order to view the presence of porosities. The resulting micrographs at a ×1000 magnification are shown in Figs 7 and 8. The micrographs show that the level of porosity at the centre of the prefoms is very low (refer to Fig. 7(a) and Fig. 8(a)), The pores appear as the black, almost round shapes on the micrographs and they act in a similar manner to second phase particles in an alloy; that is they enhance the strain hardening level. The micrographs of the edges show that the pores are elongated in the direction of material flow. The application of further loads would lead to these pores forming cracks. These micrographs highlight that the density enhancement at the centre of the preform was high and that it diminishes towards the edge of the preform.

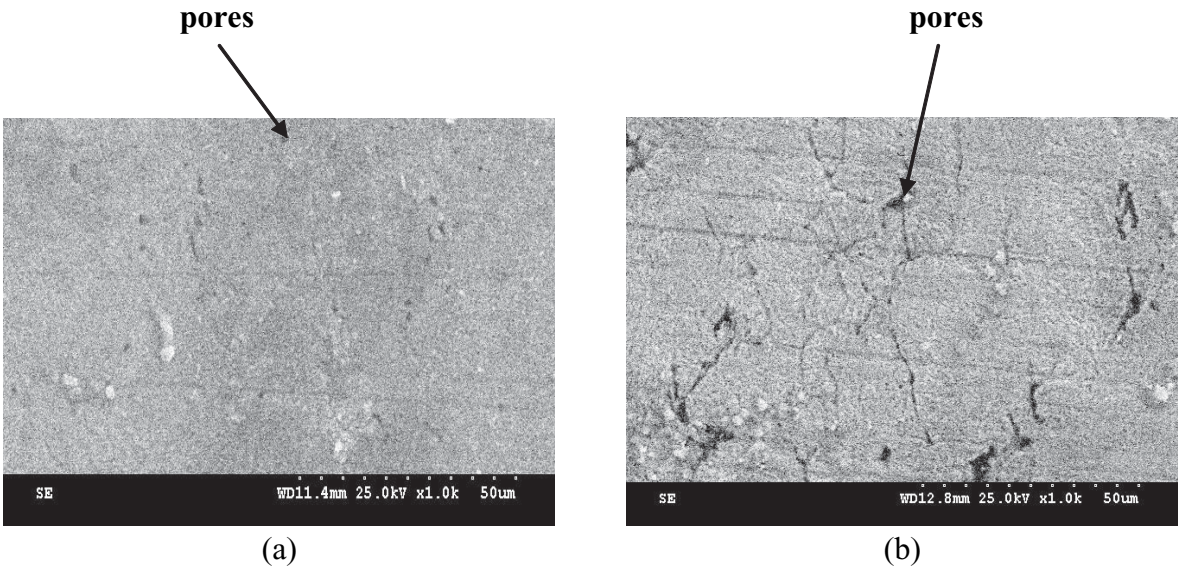

Fig. 7 Microstructure at (a) the centre and (b) the edge of the preform deformed without use of a lubricant

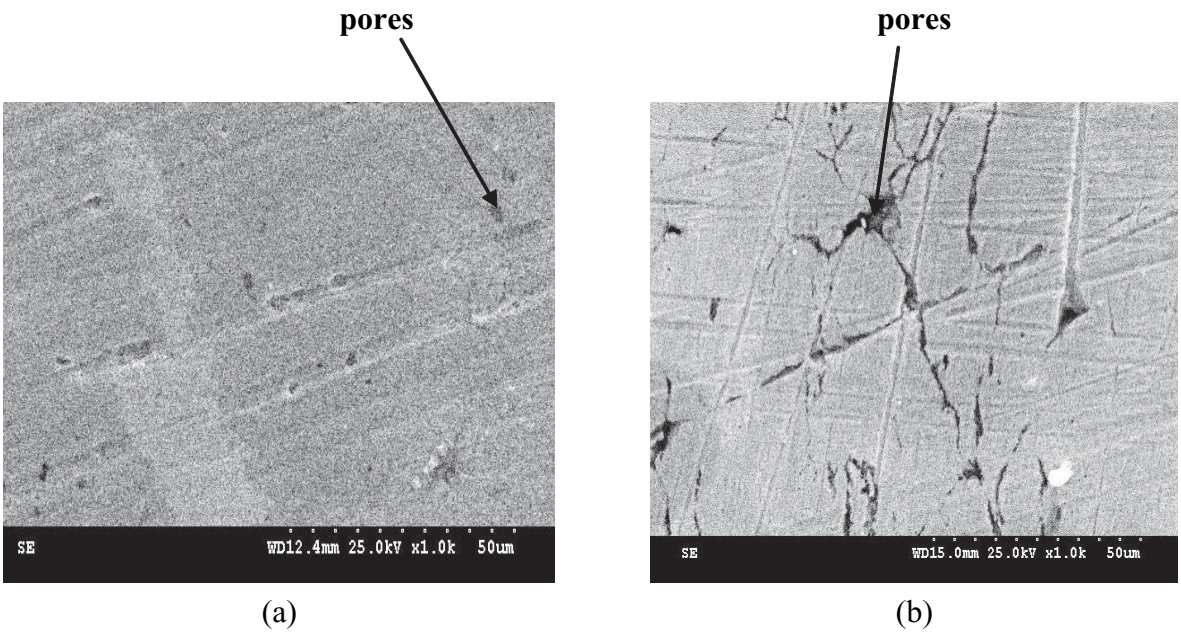

Fig. 8 Microstructure at (a) the centre and (b) the edge of the preform deformed using graphite as a lubricant

4 CONCLUSIONS

The following conclusions can be drawn from the present investigations.

1. The applied stress was continuously enhanced with an increase in the level of deformation and densification. The evolution of the stress follows three different mechanisms whether or not a lubricant is used in the experiments. The initial and final stages exhibit a high and low resistance to deformation respectively. However, in the second stage the high deformation and densification levels resulted in the stress to reaching a high steady-state value.
2. Theoretical relationships for the instantaneous strength and strain hardening were developed from the plastic flow equation for a PM preform. The strength and strain were continuously enhanced during cold upsetting. This was true whether or not a lubricant was used in the experiments; however, an increase in friction at the die contact surfaces increases the amount of work hardening created in the preform during deformation.
3. The porosity levels at the central region of the preforms are low and the pores are spherical in shape; however, at the edges of the preform the porosity level was found to be high and the pores are elongated in the material flow direction. These pores can became cracks when a suitable load is applied.

REFERENCES

1 **Šalak, A., Selecka, M.,** and **Danninger, H.** *Machinability of powder metallurgy steels*, second edition, 2005 (Cambridge International Science Publishing, Cambridge, UK).
2 **Ryuichiro, G.** Powder metallurgy growth in the automotive market. In *Business briefing: global automotive manufacturing and technology materials,* 2003, pp. 44–45 (Business Briefings Ltd, London).
3 **James, W. B.** and **West, G. T.** Powder metal technologies and application. In *ASM handbook*, volume 7, 2002, pp. 751–768 (ASM, Metals Park, Ohio).
4 **Rahman, M. A.** and **El-Sheikh, M. N.** Workability in forging of powder metallurgy compacts. *J. Mater. Process. Technol.*, 1995, **54**, 97–102.
5 **Rajeshkannan, A., Pandey, K. S., Shanmugam, S.,** and **Narayanasamy, R.** Some studies on barrelling of powder preforms during cold upsetting. *J. Mech. Behav. Mater.*, 2006, **17**(6), 415–430.
6 **Saranjit, S.** and **Jha, A. K.** Analysis of dynamic effects during high speed forging of sintered preforms. *J. Mater. Process. Technol.*, 2001, **112**(1), 53–62.
7 **Rao, K. P.** and **Hawbolt, E. B.** Development of constitutive relationships using compression testing of a medium carbon steel. *J. Mater. Process. Technol.*, 1992, **114**(1), 116–123.
8 **Saurabh, G., Venkata, N. R.,** and **Dixit, P. M.** Ductile fracture prediction in axisymmetric upsetting using continuum damage mechanics. *J. Mater. Process. Technol.*, 2003, **141**(2), 256–265.
9 **Seetharaman, V., Doraivelu, S. M.,** and **Gegel, H. L.** Plastic deformation behavior of compressible solids. *J. Mater. Shap. Technol.*, 1990, **8**(4), 239–248.
10 **Stefan, S.** Analysis of densification and strains in the uniaxial compression of sintered materials. *J. Mater. Process. Technol.*, 1992, **34**(1–4), 365–372.
11 **Selvakumar, N., Radha, P., Naryanasamy, R.,** and **Joseph, M. D.** Prediction of deformation characteristics of sintered aluminium preforms using neural networks. *Model. Simul. Mater. Sci. Engng.*, 2004, **12**, 611–620.
12 **Lee, S. C.** and **Kim, K. T.** Densification behavior of aluminum alloy powder under cold compaction. *Int. J. Mech. Sci.*, 2002, **44**(7), 1295–1308.
13 **Kandavel, T. K., Chandramouli, R.,** and **Shanmugasundram, D.** Experimental study of the plastic deformation and densification behaviour of some sintered low alloy P/M steels. *Mater. Des.*, 2009, **30**(5), 1768–1776.
14 **Cheng-Chao, H.** and **Jung-Ho, C.** An investigation into the forming limits of sintered porous materials under different operational conditions. *J. Mater. Process. Technol.*, 2004, **148**(3), 382–393.
15 **Senthilkumar, V., Naryanasamy, R.,** and **Pandey, K. S.** Effect of initial preform geometry and friction on the cold deformation behaviour of sintered titanium carbide composite steel. *Int. J. Mater. Form.*, 2008, **1**(4), 233–242.
16 **Shihao, Y., Hua, L., Yongzhi, L., Shiwei, Y.,** and **Yongjun, L.** Deformation and densification laws of powder cold forging. *J. Wuhan Univ. Technol. – Mater. Sci. Edn*, 2007, **22**(1), 17–21.
17 **Shanmugasundaram, D., Chandramouli, R.,** and **Kandavel, T. K.** Cold and hot deformation and densification studies on sintered Fe-C-Cr-Ni low alloy P/M steels. *Int. J. Adv. Mfg Technol.*, 2009, **41**(1–2), 8–15.
18 **Moyer, K. H.** Measuring density of PM materials with improved precision. *Int. J. Powder Met. Powder Technol.*, 1979, **15**, 33–42.
19 **Vamsikrishna, B., Venugopal, P.,** and **Prasad, R. K.** Analysis of deformation during simultaneous plastic deformation of dissimilar powder metallurgical preforms. *Powder Technol.*, 2004, **146**, 137–146.
20 **German, R. M.** *Powder metallurgy of iron and steel*, 1998 (Wiley, New York).
21 **Ahmed, S.** and **Agena, M.** A study of flow characteristics of nanostructured Al-6082 alloy produced ECAP under upsetting test. *J. Mater. Process. Technol.*, 2009, **209**(2), 856–863.

APPENDIX

Notation

D_f	instantaneous deformed diameter
D_0	original cross-sectional area
K	strength coefficient
K_i	instantaneous strength coefficient
n	strain hardening exponent
n_i	instantaneous strain hardening exponent
ε	true strain
σ	true stress